Mon. Not. R. Astron. Soc. **000**, 000–000 (0000) Printed 1 June 2016 (MN LATEX style file v2.2)

Wide binaries in ultra-faint galaxies: a window onto dark matter on the smallest scales

Jorge Peñarrubia[1⋆], Aaron D. Ludlow[2], Julio Chanamé[3,4], Matthew G. Walker[5]
[1]*Institute for Astronomy, University of Edinburgh, Royal Observatory, Blackford Hill, Edinburgh EH9 3HJ, UK*
[2]*Institute for Computational Cosmology, Dept. of Physics, University of Durham, South Road, Durham DH1 3LE, UK*
[3]*Instituto de Astrofísica, Pontificia Universidad Católica de Chile, Av. Vicuña Mackenna 4860, 782-0436 Macul, Santiago, Chile*
[4]*Millennium Institute of Astrophysics, Santiago, Chile.*
[5]*McWilliams Center for Cosmology, Department of Physics, 5000 Forbes Ave., Carnegie Mellon University, Pittsburgh, PA 15213, USA*

arXiv:1605.09384v1 [astro-ph.GA] 30 May 2016

1 June 2016

ABSTRACT

We carry out controlled N-body simulations that follow the dynamical evolution of binary stars in the dark matter (DM) haloes of ultra-faint dwarf spheroidals (dSphs). We find that wide binaries with semi-major axes $a \gtrsim a_t$ tend to be quickly disrupted by the tidal field of the halo. In smooth potentials the truncation scale, a_t, is mainly governed by (i) the mass enclosed within the dwarf half-light radius (R_h) and (ii) the slope of the DM halo profile at $R \approx R_h$, and is largely independent of the initial eccentricity distribution of the binary systems and the anisotropy of the stellar orbits about the galactic potential. For the reported velocity dispersion and half-light radius of Segue I, the closest ultra-faint, our models predict a_t values that are a factor 2–3 smaller in cuspy haloes than in *any* of the cored models considered here. Using mock observations of Segue I we show that measuring the projected two-point correlation function of stellar pairs with sub-arcsecond resolution may provide a useful tool to constrain the amount and distribution of DM in the smallest and most DM-dominated galaxies.

Key words: Galaxy: kinematics and dynamics; galaxies: evolution.

1 INTRODUCTION

The distribution of mass on very small galactic scales can be used to test a large range of dark matter (DM) models. DM made of 'cold' and collisionless particles clusters on virtually all scales, virializing into equilibrium DM haloes whose density profiles diverge toward the centre as $\rho \sim r^{-1}$ (e.g. Dubinski & Carlberg 1991; Navarro, Frenk & White 1996). In contrast, DM haloes made of warm or self-interacting particles follow homogeneous-density profiles with a 'core' size that depends on the particle mass (Bode et al. 2001) or cross-section (e.g. Zavala et al. 2013). Recently, ultra-light axion-particles have attracted considerable attention as they can provide large cores and solve the over-abundance problem simultaneously (e.g. Marsh & Pop 2015 and refs. therein). In addition, Lombriser & Peñarrubia (2015) show that cosmological scalar fields that couple non-minimally to matter may lead to the inference of DM cores in dwarf spheroidal galaxies (dSphs).

Observationally, the distribution of DM in the Milky Way dSphs is a matter of ongoing debate. Although current constraints favour cored halo models in at least two of the brightest ($L \sim 10^7 L_\odot$) dwarfs (Walker & Peñarrubia 2011), baryonic feedback may have modified the primordial DM distribution in these systems, greatly complicating the interpretation of inferred halo profiles (e.g. Pontzen & Governato 2012). Even if it is becoming progressively clear that faint ($L \lesssim 10^6 L_\odot$) dSphs cannot generate sufficient feedback energy to remove the primordial CDM cusps (Peñarrubia et al. 2012, di Cintio et al. 2014), the small number of chemodynamical tracers in these galaxies and the existence of model degeneracies introduces severe uncertainties in equilibrium modelling techniques (Breddels & Helmi 2013). As a result, alternative means of constraining the DM distribution in faint dSphs are needed. Along this line Errani et al. (2015) showed that the internal kinematics of stellar streams associated with dSphs encode information on the progenitor's DM halo profile.

In this paper we show that wide binary stars may offer an alternative route to probe the DM potential of the Milky Way ultra-faint ($L \lesssim 10^4 L_\odot$) dSphs. Due to their low binding energies wide binaries are easily disrupted by the host tidal field (Heggie 1975), which we assume to be completely DM-dominated during the full dynamical history of these objects. In §2 we describe the equations of motion that govern the evolution of binary systems in dSphs. §3 outlines the N-body experiments, which are later used in §4 to generate mock data and explore observational signatures. The results are summarized in §5.

⋆ jorpega@roe.ac.uk

2 BINARY SYSTEMS IN A GALACTIC POTENTIAL

2.1 Equations of motion

Consider two stars in a binary system with masses m_1 and m_2 and a relative separation $\mathbf{r} = \mathbf{R}_1 - \mathbf{R}_2$ moving in a galactic (spherical) potential $\Phi_G(R)$. In the galactic rest frame their barycentre can be calculated as $\mathbf{R} = (m_1\mathbf{R}_1 + m_2\mathbf{R}_2)/m_b$, where $m_b = m_1 + m_2$ is the mass of the binary system and

$$\begin{aligned} \mathbf{R}_1 &= +\frac{m_2}{m_1+m_2}\mathbf{r}+\mathbf{R} \\ \mathbf{R}_2 &= -\frac{m_1}{m_1+m_2}\mathbf{r}+\mathbf{R}. \end{aligned} \tag{1}$$

Hence, the equations of motion can be written as

$$\begin{aligned} \ddot{\mathbf{R}}_1 &= -\frac{Gm_2}{|\mathbf{R}_1-\mathbf{R}_2|^3}(\mathbf{R}_1-\mathbf{R}_2) - \nabla\Phi_G(\mathbf{R}_1) = -\frac{Gm_2}{r^3}\mathbf{r} - \nabla\Phi_G(\mathbf{R}_1) \\ \ddot{\mathbf{R}}_2 &= -\frac{Gm_1}{|\mathbf{R}_2-\mathbf{R}_1|^3}(\mathbf{R}_2-\mathbf{R}_1) - \nabla\Phi_G(\mathbf{R}_2) = +\frac{Gm_1}{r^3}\mathbf{r} - \nabla\Phi_G(\mathbf{R}_2). \end{aligned} \tag{2}$$

In this work we shall assume that the relative separation between the stars is much smaller than their distance to the galaxy centre, such that $r/R \ll 1$. Inserting Equation (1) into (2) and Taylor expanding $\nabla\Phi_G$ around the barycentre, $\mathbf{R}$, yields an equation of motion for the relative separation between the pair

$$\ddot{\mathbf{r}} = \ddot{\mathbf{R}}_1 - \ddot{\mathbf{R}}_2 \approx -\frac{Gm_b}{r^3}\mathbf{r} + \mathbf{T}\cdot\mathbf{r}; \tag{3}$$

where $\mathbf{T}$ is the *tidal tensor*, defined

$$T^{ij} = -\left.\frac{\partial^2\Phi_G}{\partial x_i \partial x_j}\right|_{\mathbf{R}}. \tag{4}$$

Since T^{ij} is symmetric, it has only 6 independent components.

To compute the separation at which the mutual gravitational attraction between the stars becomes comparable to the strength of the external tidal field it is useful to consider the case of a binary system moving on a circular orbit with an angular frequency $\Omega = v_c/R = [GM_G(<R)/R^3]^{1/2}$ about a host galaxy with a mass profile $M_G(R)$. Following Renaud, Gieles & Boily (2011) we rotate the binary frame to a new coordinate system $\mathbf{r}' = (x', y', z')$, where x' is parallel to $\mathbf{R}$, y' is parallel to $\dot{\mathbf{R}}$, and z' is perpendicular to both x' and y'. In these coordinates the effective tidal tensor $T_e = -\partial^2(\Phi_G + \Phi_c)/(\partial x_i \partial x_j)$ contains a centrifugal potential $\Phi_c = -\Omega^2 r^2/2$. The eigenvalue of T_e associated with the x'-axis (λ_1) determines the location of the Lagrange points L1 and L2 and defines the *tidal radius* (Renaud et al. 2011)

$$r_t \equiv \left[\frac{Gm_b}{\lambda_1}\right]^{1/3}, \tag{5}$$

where

$$\lambda_1 = -\left.\frac{\partial^2\Phi_G}{\partial x'^2}\right|_{\mathbf{R}'} + \left.\frac{\partial^2\Phi_G}{\partial z'^2}\right|_{\mathbf{R}'} \approx \gamma\Omega^2, \tag{6}$$

and $\gamma(R) \equiv -\mathrm{d}\log\rho/\mathrm{d}\log R$ is the power-law slope of the host's density profile computed at the galactocentric radius R. Note that in a Keplerian potential $\gamma = 3$ and $\Omega^2 = GM_G/R^3$, which recovers the well-known Jacobi radius $r_t = R[m_b/(3M_G)]^{1/3}$.

Binary systems with separations $r \gtrsim r_t$ may be disrupted by the host tidal field. Interestingly, Eqs. (5) and (6) imply that the tidal radius diverges in the limit $\gamma \to 0$, suggesting that tidal disruption will be less efficient in galaxies with shallow density profiles[1].

[1] Indeed, harmonic potentials have a *compressive* tidal field where all the eigenvalues become negative (see Renaud et al. for details).

2.2 Dwarf spheroidal galaxies

Dwarf spheroidal galaxies (dSphs) are particularly interesting objects because their gravitational potential is completely DM dominated, i.e. $\Phi_G = \Phi_{\rm baryons} + \Phi_{\rm DM} \approx \Phi_{\rm DM}$ (e.g. Mateo 1998; Gilmore et al. 2007). Hence, measuring the relative separation between resolved stellar pairs in these galaxies can potentially be used to constrain the DM potential.

For simplicity, we assume that binary systems form with a single mass m_b and initially follow the same spatial distribution as the total stellar component, $\rho_\star(R)$, with a half-light radius, R_h. Eqs. (5) and (6) indicate that the disruption of binary systems due to tides will be mainly determined by (i) the slope of the DM density profile at $R \approx R_h$ and (ii) the enclosed mass $M(<R_h)$. Several studies have shown that the latter quantity can be robustly inferred from observations as

$$M(<R_h) = \frac{5R_h\sigma_\star^2}{2G}, \tag{7}$$

where $\sigma_\star$ is the luminosity-averaged velocity dispersion (Walker et al. 2009). The mass estimate (7) is independent of the stellar velocity anisotropy (e.g. Walker et al. 2009) and also holds in triaxial haloes drawn from cosmological simulations (Laporte et al. 2013).

To estimate the tidal radius (5) for the Milky Way dSph population we use the observed relationship between the velocity dispersion and half-light radius, $\sigma_\star = \sigma_0(R_h/R_0)^\alpha$, where $\alpha \simeq 0.5$, $\sigma_0 \simeq 0.93\,\mathrm{km\,s^{-1}}$ and $R_0 = 1\,\mathrm{pc}$ (Walker et al. 2010). Combination of Eqs. (5), (6) and (7) for $m_b = 1M_\odot$ yields

$$r_t = \left[\frac{2Gm_bR_0^{2\alpha}}{5\gamma\sigma_0^2}\right]^{1/3} R_h^{2(1-\alpha)/3} \simeq 0.27\,\mathrm{pc}\left[\frac{1}{\gamma(R_h)}\cdot\frac{R_h}{10\,\mathrm{pc}}\right]^{1/3}, \tag{8}$$

which suggests that binary disruption by the smooth DM tidal field is most efficient in the smallest dSphs. Given that the widest binary known to us has a separation of $\sim 1.1\,\mathrm{pc}$ (Chanamé & Gould 2004; Quinn et al. 2009), galaxies with half-light radii $R_h \lesssim 700\,\mathrm{pc}$ provide the best targets to probe the shape of the DM halo mass profile via the separation function of stellar pairs (see §4.2).

3 *N*-BODY EXPERIMENTS

The tidal limit estimates derived in §2.2 assume that stars move on circular orbits about the centre of the potential. In this Section we use N-body techniques to examine more realistic orbital configurations that reproduce the brightness profile and velocity dispersion of Segue I, the closest ultra-faint dSph known to us.

3.1 Evolution in the host galaxy potential

We use the method of Walker & Peñarrubia (2011) to generate tracer particle ensembles in equilibrium within a spherical DM halo potential (see that paper for details). Briefly, we adopt a DM model

$$\rho(R) = \frac{\rho_0 R_s^4}{(R+R_c)(R+R_s)^3}; \tag{9}$$

which approaches a Hernquist (1990) profile in the limit $R_c \to 0$, thus recovering the cuspy profile observed in self-consistent CDM simulations of structure formation.

Stars are tracer particles distributed as a Plummer (1911) sphere,

$$\rho_\star(R) = \frac{\rho_{\star,0}}{[1+(R/R_\star)^2]^{5/2}}; \tag{10}$$

where $R_h \simeq 1.3R_\star$. Stellar velocities are drawn from a Opsikov-Merrit distribution function (Osipkov 1979; Merrit 1985). These models have velocity distributions with anisotropy profiles of the form $\beta_\star(R) \equiv 1-\overline{v_\theta^2}/\overline{v_r^2} = R^2/(R^2+R_a^2)$, where R_a is the "anisotropy radius". Here we consider stellar models with isotropic ($R_a \to \infty$) and radially anisotropic ($R_a = R_\star$) orbital distributions.

The model parameters are chosen to reproduce the luminosity profile and the velocity dispersion of Segue I (Belokurov et al. 2007), the closest ultra-faint dSph ($D = 23$ kpc, Martin et al. 2008). Inserting the (deprojected 3D) half-light radius $R_h \simeq 40$ pc (Martin et al. 2008; Simon et al. 2011) and the velocity dispersion $\sigma_\star \simeq 4\,\mathrm{km\,s^{-1}}$ (Geha et al. 2009; Simon et al. 2011) in Eq. (7) leads to an enclosed mass $M(<R_h) \simeq 3\times10^5 M_\odot$ which, combined with a luminosity $L_v \sim 300 L_\odot$, yields a mass-to-light ratio $2M(<R_h)/L \sim 2000(M_\odot/L_\odot)$, making this galaxy one of the darkest known to us (Geha et al. 2009). Note that the dynamical time of this galaxy, $\Omega^{-1} \simeq 7$ Myr, is hundreds of times shorter than the the estimated stellar age (Belokurov et al. 2007). To find the DM parameters ρ_0 and R_s we impose two conditions on the halo profile: (i) the mass enclosed within 40 pc is $3\times10^5 M_\odot$ and (ii) its concentration follows the relation found by Macciò et al. (2007) at redshift $z = 0$. Tests with different $M-c$ relations yield very similar results, highlighting the fact that at leading order the tidal field is controlled by $M(<R_h)$ and γ, as expected from (6). We consider DM core sizes $R_c/R_h = 0, 1, 2$ and 3 ($R_c = 0$ corresponds to a DM cusp). With these choices the halo parameters are $[R_c/\mathrm{pc}, R_s/\mathrm{pc}, \rho_0/(M_\odot\,\mathrm{pc}^{-3})] = [0, 85, 0.95]; [40, 300, 0.42]; [80, 913, 0.18]$ and $[120, 2465, 0.09]$. All our models have scale radii $R_s \gg R_c \sim R_h$, so that the stellar populations are deeply embedded in the DM halo potential.

For each halo model we generate equilibrium ensembles of $N_\star = 10^4$ tracer particles. Orbits in the host potential are followed for 10 Gyr using the particle-mesh code SUPERBOX (Fellhauer et al. 2000) with a time step $\Delta t = \Omega^{-1}/20$. For Seg I $\Omega^{-1} \simeq 7$ Myr, which yields a total number of time steps $N_t = 10\,\mathrm{Gyr}/\Delta t = 28570$. At each timestep, and for all particles, we record the 6 (independent) components of the tidal tensor (4).

The equations of motion (3) are solved using a Runge-Kutta scheme (e.g. Press et al. 1992) with a variable time-step chosen such that energy conservation in isolation is better than 1 : 1000. To calculate the tidal force at any arbitrary time of the binary evolution we use a sync-interpolation algorithm (Peñarrubia et al. *in prep.*).

3.2 Binary systems

We characterize the initial orbits of binary systems by their semi-major axis distribution $q(a, t = 0)$, and a eccentricity distribution $f(e, t = 0)$. Both are probability functions normalized so that $\int_{a_{\rm min}}^{a_{\rm max}} q(a)da = \int_0^1 f(e)de = 1$ at all times.

Motivated by observations of wide binaries in the Milky Way we adopt a power-law distribution $q(a, t = 0) = c_\lambda a^{-\lambda}$, with c_λ being a normalization constant and $\lambda \gtrsim 1$. Current constraints favour a power-law index between $\lambda = 1$ (the Öpik 1924 distribution; e.g. Longhitano & Binggeli 2010) and $\lambda \simeq 1.5$ (e.g. Chanamé & Gould 2004); for simplicity the results shown below assume $\lambda = 1$, although we also test models with $\lambda = 1.5$ Below we show that the limits $a_{\rm min} = 0.02$ pc and $a_{\rm max} = 2.0$ pc cover the relevant scales in our study. For a pair with $m_b = 1M_\odot$ this implies orbital periods between 0.26–264 Myr.

The eccentricity distribution of binaries with $a \gtrsim 0.05$ pc remains largely unconstrained. Recently, Tokovinin & Kiyaeva (2016) find that nearby binaries with $a \lesssim 0.05$ pc have a distribution $f(e) \propto \kappa e$, with $\kappa \approx 1.2$. N-body simulations that follow the formation of wide binaries during the dissolution of stellar clusters find $\kappa \simeq 2$ (Kouwenhoven et al. 2010). Here we explore models with random ($f(e) = $ const.) and thermal ($\kappa = 2$) distributions.

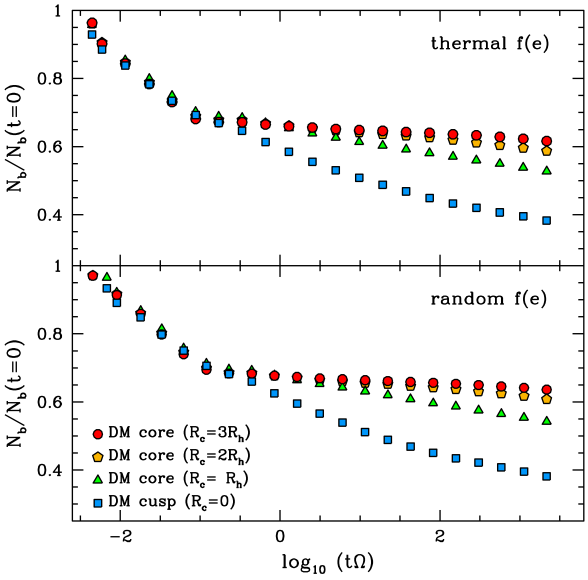

Figure 1. Fraction of surviving binaries as a function of time. Note the two distinct evolutionary regimes, a rapid 'catastrophic' evolution where tidal disruption occurs on a time-scale comparable to the orbital dynamical time of the galaxy, $t \sim \Omega^{-1}$, followed by a much slower 'diffusive' evolution on time-scales $t \gg \Omega^{-1}$. Comparison between the two panels indicates no sensitivity to the initial eccentricity distribution, $f(e)$.

4 RESULTS

4.1 Tidal disruption

Fig. 1 shows that the disruption of binary systems is less efficient in haloes with shallow density profiles, as expected from the analytical estimates in §2.1. The binary fraction follows two evolutionary regimes: an exponential disruption rate on a time-scale comparable to the orbital dynamical time of the galaxy, $t \sim \Omega^{-1}$, in which binaries are disrupted shortly before or during their first pericentric approach. This is followed by a very gentle decline on time-scales $t \gg \Omega^{-1}$ resulting from small ('diffusive') energy injections during consecutive pericentres. Comparison of the upper and lower panels shows that the initial eccentricity distribution plays a minor role in determining the survival of wide binaries. In what follows we focus on models with a thermal eccentricity distribution.

Given that the binding energy of a binary system is $E = -Gm_b/(2a)$ we expect tidal disruption to affect predominantly systems with large semi-major axes. This is visible in Fig. 2, which shows that the fraction of surviving binaries, $f_s \equiv q(a,t)/q(a,t=0)$, sharply drops at semi-major axes $a \gtrsim a_t$ (marked with vertical dotted lines for ease of reference), with a truncation a_t that shifts to larger separations as the DM core size increases relative to the stellar size. In contrast, binaries with $a \ll a_t$ and high binding energies survive regardless of the halo profile. To estimate a_t we fit f_s with a broken power-law function,

$$g(a) = \frac{1}{[1+(a/a_t)^m]^{n/m}}, \qquad (11)$$

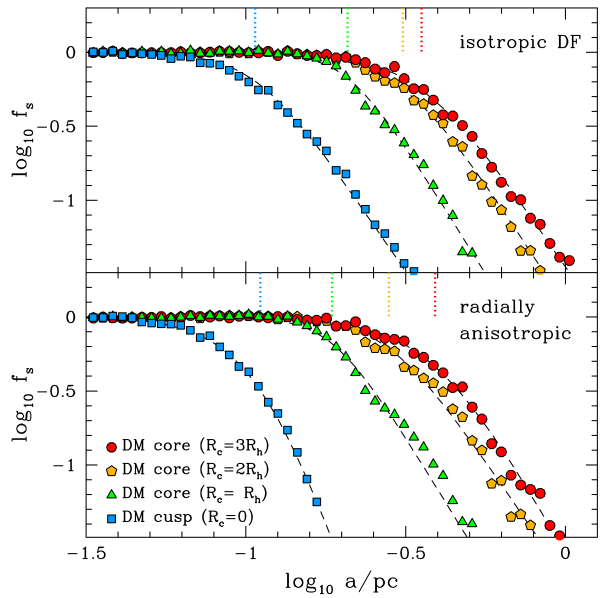

Figure 2. Fraction of surviving binaries as a function of semi-major axis. Upper and lower panels show stellar binaries with isotropic ($R_a \to \infty$) and radially anisotropic ($R_a = R_\star$) orbital distributions (see text). Black-dashed lines show the best-fitting functions (11). Vertical dotted lines mark the location of the truncation scale a_t.

which contains three free parameters: a truncation a_t, an intermediate slope $m > 0$ and an outer slope $n \geq 0$, such that $f_s \sim (a/a_t)^{-n}$ for $a \gg a_t$. For stellar binaries moving on isotropic orbits ($R_a \to \infty$; upper panel) the best-fitting parameters are $[a_t/\,\mathrm{pc}, m, n] = [0.11, 4.7, 3.2], [0.21, 5.9, 3.5], [0.31, 4.1, 3.4]$, $[0.36, 3.8, 3.2]$ for $R_c/R_h = 0, 1, 2$ and 3, respectively; for radially anisotropic models ($R_a = R_\star$; lower panel) we find $[0.11, 3.8, 6.3], [0.19, 5.9, 3.5], [0.28, 4.6, 3.2]$ and $[0.39, 3.5, 3.9]$, respectively. We checked that these values do not depend on the slope of $q(a, t = 0)$ insofar as $\lambda \lesssim n$. We also find a negligible dependence to the initial eccentricity distribution, $f(e, t = 0)$. Radially anisotropic orbital distributions bring a larger fraction of binaries to the central regions of the potential. For cuspy profiles this leaves a_t unchanged, but steepens the power-law index n. For cored models, however, the shape of the binary separation function is largely independent of the assumed velocity distribution. The key result is that f_s depends sensitively on the DM profile: in cuspy haloes f_s is truncated at separations a factor of 2–3 smaller than in *any* of the cored profiles considered here, reflecting the weak dependence of the tidal radius (5) on galactocentric distance in regions where the halo slope $\gamma \to 0$.

4.2 Observational signatures

A direct measurement of the orbital parameters of wide binaries in dSphs is currently unfeasible owing to their long orbital periods. To investigate whether the *projected* separation of stellar pairs holds information on the shape of the DM halo profile we construct mock catalogues of Segue I using the isotropic N-body models outlined in §3. The number of stars in this galaxy is $N_{\star,\rm tot} \approx \Upsilon_\star L_v/\langle m_\star\rangle = 1500$, where we have assumed a stellar mass-to-light ratio $\Upsilon_\star = 2 M_\odot/L_\odot$ typical for old, metal-poor stellar populations (Bell & de Jong 2001), and a Kroupa (2002) IMF with a mean stellar mass $\langle m_\star\rangle = 0.4 M_\odot$. We further assume that at most $2/3$ of $N_{\star,\rm tot}$ can be detected with current instrumentation, which yields $N_\star = 1000$, of which $N_b = f_b N_\star$ are individual particles in binary systems with locations given by Eq. (1) with $m_1 = m_2$. For each mock we measure the projected two-point correlation function (2PCF) as

$$1 + w(s) \equiv \frac{\psi(s)}{P(s)}, \tag{12}$$

where $\psi(s)$ is the number of pairs with projected separations between $s, s + \mathrm{d}s$ and $P(s)$ is the expected number of *random* pairs in the same interval.

As expected, Fig. 3 shows that presence of binaries leads to an *excess* ($w > 0$) of pairs at separations $s \lesssim a_t$ with respect to the random distribution. To understand the shape of the 2PCF we can relate the function $\psi(s)$ to the semi-major axis distribution $q(a, t)$ as (Longhitano & Binggeli 2010)

$$\psi(s) \approx f_b N_\star q(\langle s\rangle, t) = f_b N_\star c'_\lambda \langle s\rangle^{-\lambda} f_s(\langle s\rangle, t), \tag{13}$$

where $\langle s\rangle$ is the average projected separation at a fixed semi-major axis, $f_s \approx g$ is the survival fraction curves fitted in Fig. 2 (dashed lines), and c'_λ is a normalization factor such that $\int_{\langle s\rangle_{\rm min}}^{\langle s\rangle_{\rm max}} \mathrm{d}s q(s, t) = 1$. For a thermal eccentricity distribution $\langle s\rangle = 5\pi a/16 \simeq 0.98 a$ (Yoo et al. 2004). However, our N-body models indicate that the orbits of bianary systems with $a \gtrsim a_t$ become radially biased, decreasing the average separation to $\langle s\rangle/a = 0.93$ and 0.70 in cuspy and cored ($R_c = 3R_h$) halo models, respectively. Blue-solid and red-dashed lines in Fig. 3 show that Eq. (13) provides a good match to the measured 2PCFs. Note that at $s \ll a_t$ we have $f_s \simeq 1$ and $\psi(s) \sim s^{-\lambda}$. Since the number of random pairs obeys $P(s)\mathrm{d}s \sim s\mathrm{d}s$, we find that $w \sim s^{-(\lambda+1)}$ at small separations, thus constraining the slope of the *unperturbed* semi-major axis distribution (λ). In addition, theoretical lines cross each other at $s \sim a_t$, and since $q(a, t)$ is normalized to unity we find that the smaller the truncation scale the larger contribution to w at small separations and *vice versa*, suggesting that the 2PCF provides a useful statistical tool to distinguish between the halo profiles explored in §3. Whether or not a statistically-meaningful distinction is feasible with current technology depends on the (unknown) wide binary fraction. The Poisson error bars indicate that a robust characterization of the DM halo profile in galaxies with $L \lesssim 10^3 L_\odot$ at a heliocentric distance D requires deep astrometry data with a minimum resolution $\Delta\theta_{\rm min} \sim a_t/D$ and $f_b \gtrsim 0.1$.

5 DISCUSSION & SUMMARY

In this paper we use N-body simulations to explore the survival of wide stellar binaries in the DM haloes of ultra-faint dSphs. We find that binaries with semi-major axes $a \gtrsim a_t$ are disrupted by the halo tidal field on time-scales $t \sim \Omega^{-1} = [GM(< R_h)/R_h^3]^{-1/2}$, where $M(< R_h)$ is the mass enclosed within the half-light radius R_h of the dwarf. Our models indicate that the truncation scale a_t is sensitive to the shape of the DM halo mass profile. For the dynamical mass ($\simeq 3 \times 10^5 M_\odot$), size ($\simeq 40\,$pc) and stellar ages ($\gtrsim 10\,$Gyr) of Segue I, the closest ultra-faint, our models predict values for a_t that are a factor of 2–3 smaller in cuspy haloes than in any of the cored models considered here.

The models adopt a static, smooth DM potential in order to derive the dSph tidal field acting on the binary particles. Although the static approximation may be justified by the small evolution of DM haloes within the region populated by stars (e.g. Cuesta et al. 2008), neglecting the large population of dark substructures predicted by ΛCDM may overestimate the survival of binaries (Peñarrubia et

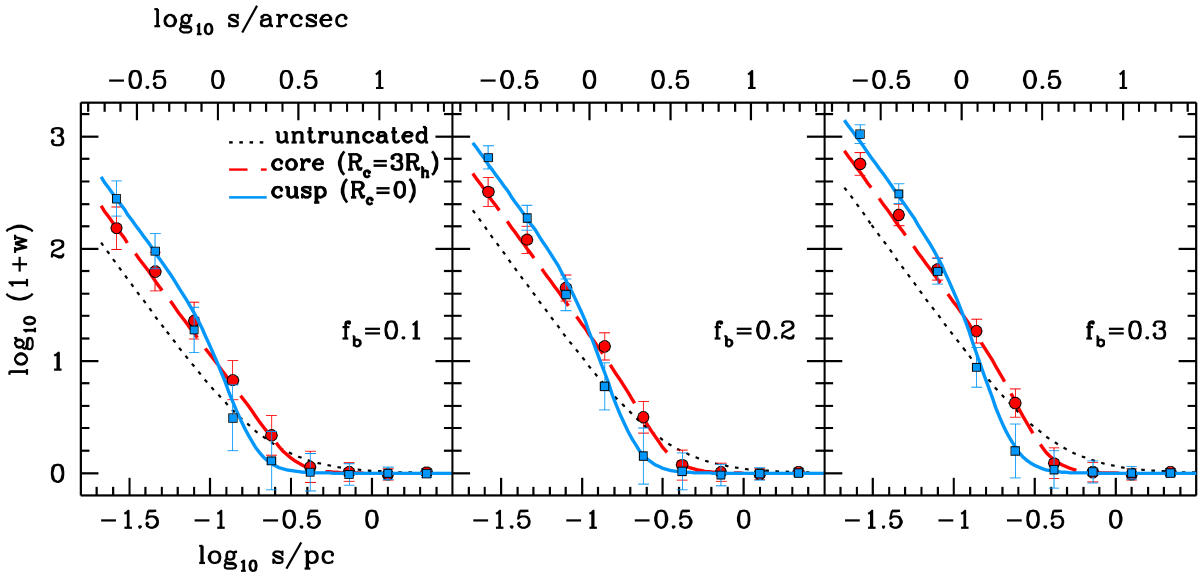

Figure 3. Projected two point correlation function for mocks of Segue I with $N_\star = 1000$ and different wide binary fractions ($f_b = N_b/N_\star$). Blue-solid and red-dashed lines correspond to the analytical estimates from Equation (13). Comparison with Fig. 2 shows that theoretical lines cross each other at $s \sim a_t$.

al. 2010). Dense substructures (both dark and baryonic) may be particularly damaging if they can reach the central regions of the host halo before being tidally disrupted (Laporte & Peñarrubia 2015; Starkenburg & Helmi 2015; Benítez-Llambay et al. 2016). Given that dynamical friction becomes inefficient in homogeneous-density cores (Read et al. 2006) we expect encounters between stars and substructures to be more likely in dSphs embedded in cuspy DM haloes. Studying the impact of clumps may also be relevant for warm and axion dark matter models in which dSphs are expected to be largely devoid of dark substructures. We plan to address these issues in future contributions by injecting binary populations in potentials drawn from cosmological hydrodynamic simulations.

The analysis of mock data indicates that measuring the 2PCF of stellar pairs in the Milky Way ultra-faint dSphs may provide a useful statistical tool to detect and characterize the semi-major distribution of wide binaries, and hence constrain the inner slope of the DM halo profile. This type of analysis requires deep photometric data with sub-arcsecond resolution, providing a case for space missions like HST and the forthcoming WFIRST.

6 ACKNOWLEDGEMENTS

We thank the referee F. Renaud for his insightful comments. ADL is supported by a COFUND Junior Research Fellowship. JC acknowledges support from Proyecto FONDECYT Regular 1130373; BASAL PFB-06 Centro de Astronomía y Tecnologías Afines; and by the Chilean Ministry for the Economy, Development, and Tourism's Programa Iniciativa Científica Milenio grant IC 120009, awarded to the Millennium Institute of Astrophysics. MGW is supported by NSF grants AST-1313045 and AST-1412999.

REFERENCES

Bell, E. F., & de Jong, R. S. 2001, ApJ, 550, 212
Belokurov, V., et al. 2007, ApJ, 654, 897
Benítez-Llambay, et al. 2016, MNRAS, 456, 1185
Bode, P., Ostriker, J. P., & Turok, N. 2001, ApJ, 556, 93
Breddels, M. A., & Helmi, A. 2013, A&A, 558, A35
Chanamé, J., & Gould, A. 2004, ApJ, 601, 289
Cuesta, A. J., Prada, F., Klypin, A., & Moles, M. 2008, MNRAS, 389, 385
Di Cintio, et al. 2014, MNRAS, 437, 415
Dubinski, J., & Carlberg, R. G. 1991, ApJ, 378, 496
Errani, R., Peñarrubia, J., & Tormen, G. 2015, MNRAS, 449, L46
Fellhauer, M., et al. 2000, New Astronomy, 5, 305
Geha, M., et al. 2009, ApJ, 692, 1464
Gilmore, G., et al. 2007, Nuclear Physics B Proceedings Supplements, 173, 15
Heggie, D. C. 1975, MNRAS, 173, 729
Hernquist, L. 1990, ApJ, 356, 359
Kouwenhoven, M. B. N., et al. 2010, MNRAS, 404, 1835
Kroupa, P. 2002, Science, 295, 82
Laporte, C. F. P., Walker, M. G., & Peñarrubia, J. 2013, MNRAS, 433, L54
Laporte, C. F. P., & Peñarrubia, J. 2015, MNRAS, 449, L90
Longhitano, M., & Binggeli, B. 2010, A&A, 509, A46
Lombriser, L., & Peñarrubia, J. 2015, Phys. Rev. D, 91, 084022
Macciò, A. V., et al. 2007, MNRAS, 378, 55
Marsh, D. J. E., & Pop, A.-R. 2015, MNRAS, 451, 2479
Martin, N. F., de Jong, J. T. A., & Rix, H.-W. 2008, ApJ, 684, 1075-1092
Merritt, D. 1985, AJ, 90, 1027
Mateo, M. L. 1998, ARA&A, 36, 435
Navarro, J. F., Frenk, C. S., & White, S. D. M. 1996, ApJ, 462, 563
Öpik, E. 1924, Publ. of the Tartu Observatory, 25, 1
Osipkov, L. P. 1979, Soviet Astronomy Letters, 5, 42
Peñarrubia, J., et al. 2010, arXiv:1005.5388
Peñarrubia, J., Pontzen, A., Walker, M. G., & Koposov, S. E. 2012, ApJ, 759, L42
Plummer, H. C. 1911, MNRAS, 71, 460
Press, W. H., et al. 1992, Cambridge: University Press, 2nd ed.
Quinn, D. P., et al. 2009, MNRAS, 396, L11
Read, J. I., Goerdt, T., Moore, B., et al. 2006, MNRAS, 373, 1451

Renaud, F., Gieles, M., & Boily, C. M. 2011, MNRAS, 418, 759
Simon, J. D., Geha, M., Minor, Q. E., et al. 2011, ApJ, 733, 46
Starkenburg, T. K., & Helmi, A. 2015, A&A, 575, A59
Tokovinin, A., & Kiyaeva, O. 2016, MNRAS, 456, 2070
Walker, M. G., et al. 2009, ApJ, 704, 1274
Walker, M. G., et al. 2010, ApJ, 717, L87
Walker, M. G., & Peñarrubia, J. 2011, ApJ, 742, 20
Yoo, J., Chanamé, J., & Gould, A. 2004, ApJ, 601, 311
Zavala, J., Vogelsberger, M., & Walker, M. G. 2013, MNRAS, 431, L20